GREEN CHEMISTRY LETTERS AND REVIEWS
2025, VOL. 18, NO. 1, 2541058
https://doi.org/10.1080/17518253.2025.2541058

Design, synthesis, biological assessment, and *in silico* analysis of bisthiazolidine amide derivatives as potential anti-bacterial and anti-prostate cancer agents

Sabah Abbas[a], Ahmed A. Majed[b], Rehab G. Abood[b], Dunya AL-Duhaidahawi[c], Radwan Alanjjar[d], Huda Hadi Nameh[e], Naser A. Naser[f], Ahmed Y. Hammood[g], Mohammad Y. Alfaifi[h,i,j], Ali A. Shati[i,j], Serag Eldin I. Elbehairi[i,j], Ahmed M. Hussein[k] and Mohammed Aufy[k,l]

[a]Department of Chemistry, Education for Girls Faculty, University of Kufa, Kufa, Iraq; [b]College of Education for Pure Sciences, Department of Chemistry, Basrah University, Basrah, Iraq; [c]College of Pharmacy, University of Kufa, AL-Najaf, Iraq; [d]CADD Unit, Faculty of Pharmacy, Libyan International Medical University, Benghazi, Libya; [e]College of Pharmacy, University of Hilla, Babylon, Iraq; [f]College of Pharmacy, AL-Musaqbal University, Babylon, Iraq; [g]Department of Marine Environmental Chemistry, Marine Science Center, University of Basrah, Basrah, Iraq; [h]Central Labs, King Khalid University, Alqura'a, Abha, Saudi Arabia; [i]Biology Department, Faculty of Science, King Khalid University, Abha, Saudi Arabia; [j]Tissue Culture and Cancer Biology Research Laboratory, King Khalid University, Abha, Saudi Arabia; [k]Department of Pharmaceutical Sciences, Division of Pharmacology and Toxicology, University of Vienna, Vienna, Austria; [l]Department of Pharmaceutical Sciences, Division of Pharmaceutical Chemistry, University of Vienna, Vienna, Austria

ABSTRACT

A series of N,N′-(1,4-phenylene) bis(3-acetyl-2-arylthiazolidine-4-carboxamide) derivatives (M1-M5) was synthesized, characterized, and evaluated for antibacterial and anticancer activities. Literature from 2000 to 2023 was reviewed using PubMed and Scopus to guide compound selection. Structural characterization was confirmed via FT-IR, ^{1}H, ^{13}C-NMR, and mass spectrometry. Antibacterial activity was assessed using the disk diffusion method against *S. aureus*, *E. coli*, and *S. mutans*, with M4, M5, and M3 surpassing cefixime, exhibiting MIC values of 9.7, 39.5, and 79 µg/ML against *S. aureus*. M3 and M5 also showed notable activity against *S. mutans*. MTT assays revealed potent cytotoxicity of M4, M5, and M3 against PC3 cells, with M4 (IC50 = 19.56 µg/ML) outperforming Darolutamide drug (IC50 = 52.82 µg/ML). Molecular docking suggested EGFR inhibition. M4 induced apoptosis and G1 phase arrest in PC3 cells, demonstrating its potential as a dual-purpose therapeutic agent.

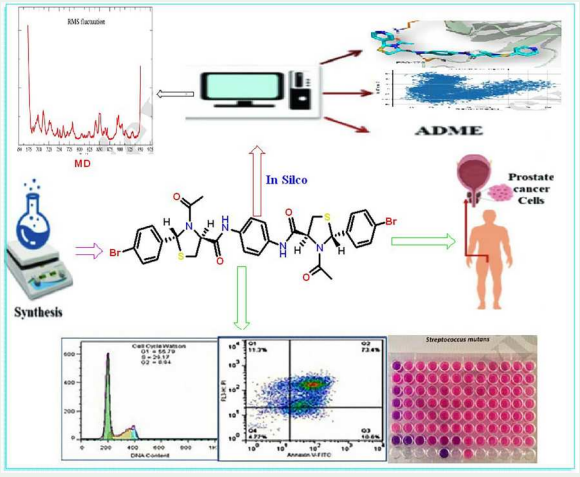

ARTICLE HISTORY
Received 29 May 2025
Accepted 24 July 2025

KEYWORDS
1,3 Thiazolidine; docking; phenylenediamine; dynamic; PC3; antibacterial; anticancer; cell cycle

CONTACT Ahmed M. Hussein ahmed.hussein@univie.ac.at, hamadaz81@gmail.com Department of Pharmaceutical Sciences, Division of Pharmacology and Toxicology, University of Vienna, Vienna, Austria; Ahmed A. Majed eduppg.ahmed.majed@uobasrah.edu.iq College of Education for Pure Sciences, Department of Chemistry, Basrah University, Basrah, Iraq

Supplemental data for this article can be accessed online at https://doi.org/10.1080/17518253.2025.2541058

1. Introduction

Prostate Cancer (PC) represents the most common malignant tumor in men worldwide, affecting the urinary tract. It is considered one of the main and influential causes of death due to delayed discovery or poor diagnosis, as well as the spread of cancer cells [1–3]. Most individuals experience apparent symptoms only in the middle or late stages of the disease, leading to wider spread. Health and nutritional care for prostate cancer patients involves the use of radiation therapy, endocrine therapy, surgical operations, or targeted chemotherapy [4,5]. Although these treatments are initially effective, they fail to halt the disease completely, often leading to its return and increased spread [6]. The most common type of prostate cancer is castration-resistant prostate cancer (CRPC), which represents a highly aggressive and metastatic malignant disease affecting the urinary tract. There are 10 million confirmed cases of prostate cancer worldwide, and despite numerous studies, developments, auxiliary factors, and treatments [7–9], controlling and treating this disease remains challenging due to severe cell resistance to various androgen (ADT) treatments, as well as resistance to the chemotherapy drug Paclitaxel [2,7]. Accumulated research has confirmed that prostate cancer can easily develop resistance to any associated protein or kinase inhibitor, limiting the effectiveness of current agents and drugs against the cells [10,11].

The development of cancer cells in general, and specifically prostate expansion, is influenced by the propagation of tumor and apoptosis cells [7]. It has been implicated in prostate cancer, necessitating the discovery of novel drugs for the treatment of this issue [12–14]. Heterocyclic compounds with an amide functional group have demonstrated a significant role in regulating normal physiological processes and targeting biological sites associated with diseases [15,16]. Amide compounds are an important class of organic compounds that have attracted considerable attention due to their distinct structure and biological effectiveness against various diseases. Examples of amid compounds are piperine (**1**, traditional medicine), Linezolid (**2**, antibacterial), and Sorafenib (**3**, anticancer) [Figure 1] [17–20].

Heterocyclic compounds also play an essential and effective role in treating numerous diseases, especially compounds containing sulfur and nitrogen, which are among the most effective due to their distinct structural composition and high ability to inhibit disease-causing cells [21]. Among others, thiadiazol, thiazolidine, and thiazole are widely explored [22,23]. The combination of amide compounds and heterocyclic compounds is important and widely applicable in the formulation of active drug-like molecules [24,25]. Some studies have demonstrated that these compounds possess biological activity and are used as antibacterial agents [26], antioxidants [27], antifungals [28], anti-inflammatory agents, and anticancer agents [29–31].

Thiazolidine compounds have been investigated, representing a heterocyclic ring containing sulfur and nitrogen. These compounds are biologically active due to their distinct structure and can be used as reliable

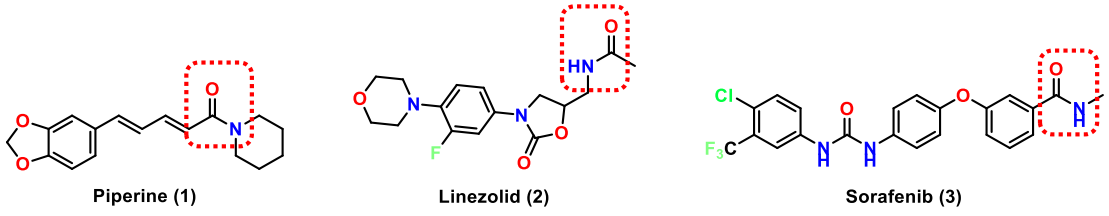

Figure 1. Examples of Drugs with amide functional group.

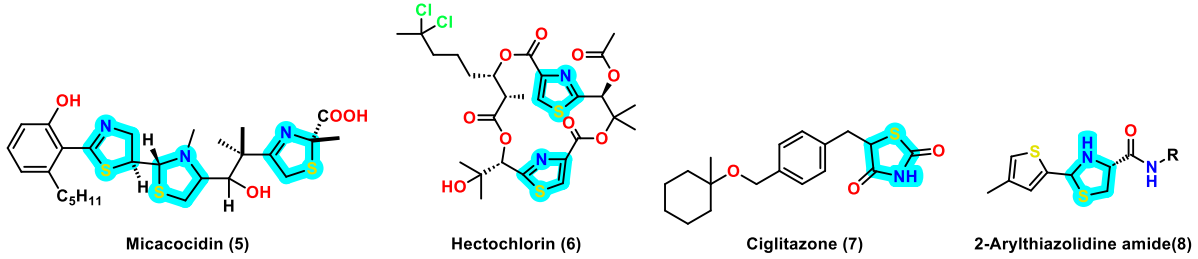

Figure 2. Thiazolidine compounds with interesting biological activities.

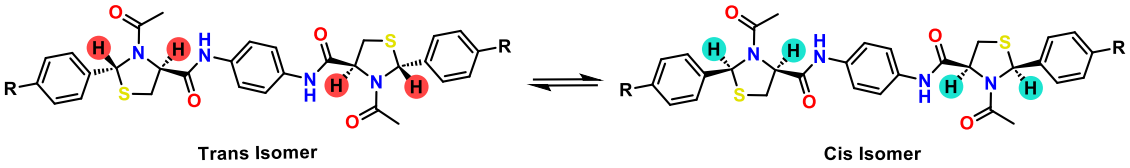

Figure 3. Possible conformation of bis amide thiazolidine derivatives.

treatments for many diseases and for regulating vital functions [32]. The activity of thiazolidine derivatives has been reported, e.g. Micacocidin drug (**5**, antibacterial), Hectochlorian (**6**, antifungal), and Ciglitazone drug (**7**, antihyperglycemic agent) [33,34], also, in the treatment of prostate cancer and in addition to its effect on apoptosis and cell cycle in mitochondria such as 2-aryl thiazolidines-4-carboxylic amide (**8**) derivates, Figure 2 [31, 33].

The human peroxisome proliferator-activated receptor gamma ($PPAR_\gamma$), a nuclear receptor that plays a key role in the regulation of cellular differentiation; in addition, $PPAR_\gamma$ is highly expressed in prostate cancer, indeed several studies showed that activation of $PPAR_\gamma$ inhibits the proliferation of prostate cancer. A ligand that activates $PPAR_\gamma$ can induce cell cycle arrest and promote apoptosis [34, 35]. The relationship between the $PPAR_\gamma$ protein and prostate cancer is multifaceted, involving the regulation of cell proliferation differentiation apoptosis. A recent study demonstrated the connection between $PPAR_\gamma$ and prostate cancer metastasis through AKT serine/ threonine kinase (AKT3), leading to a more aggressive form of the disease. The anticancer properties of $PPAR_\gamma$ activation justify the continued investigation of $PPAR_\gamma$ ligands, including phenyl thiazolidine derivatives, as potential therapeutic agents for prostate cancer [36,37].

On the other hand, epidermal growth factor receptor (EGFR) is a signaling protein extensively related to most cancer types, including prostate cancer, and is one of the most targeted proteins in cancer development and treatments. EGFR is overexpressed in prostate cancer, and it was found that EGFR can crosstalk with receptors such as the androgen receptor (AR), which is a key player in the development and progression of prostate cancer [7, 34, 36]. Thiazolidine derivatives was effective scaffolds due to their versatility in forming hydrogen bonds and hydrophobic interactions with biological targets. The rationale for selecting these specific derivatives was their potential dual activity against bacterial infections and cancer, addressing the growing demand for multifunctional therapeutics. Several studies have explored thiazolidine amide derivatives as potential anticancer, showing significant activity against prostate cancer [38], breast cancer [39]. Additionally, thiazolidine moiety act as potent, selective proapoptotic agents in several studies promoting apoptosis in cancer cells while sparing normal cells. This selective apoptosis, along with their broad anticancer activity, makes thiazolidine derivatives promising candidates for targeted cancer therapies [40].

Therefore, in this study, a series of bis thiazolidine amide derivatives were synthesized as a racemic mixture of both enantiomers [Figure 3] and were characterized using spectroscopic techniques. Their biological activity toward bacteria and PC3 cancer cells was evaluated. Finally, the possible mechanism of action of the compounds was studied *in silico* using dynamic and molecular docking.

2. Materials and methods

2.1. Materials and preparation experiments

All melting points were not corrected. IR spectrum was recorded using an (IR Shimazu) in the range of 4000-400cm^{-1}. The ^{1}H and ^{13}C NMR spectra were recorded on Brucker 400 and 100 MHz, respectively. Shifts were reported with references to the solvent DMSO-d_6 or peaks (δ H 2.5, 3.3 ppm, and δ–^{13}C 49 ppm), and *J* (coupling constant) was described in Hertz. The contractions for signal types were as follows: s for singlet, d for doublet, t for triplet, and m for multiplet. Finally, the mass spectroscopic (EI) was recorded on (an Agilent mass spectrometer – 5975 – quadrupole analyzer) in (70 eV).

Biological studies were conducted at the Pasteur Institute in Tehran, Iran. The bacterial *S. aureus* (*Staphylococcus aureus*), *E. coli* (*Escherichia coli*), and *S. mutans* (*Streptococcus mutans*) strains were sourced from the Microbiology Laboratory in the Department of Biological Evolution at the Marine Science Center, University

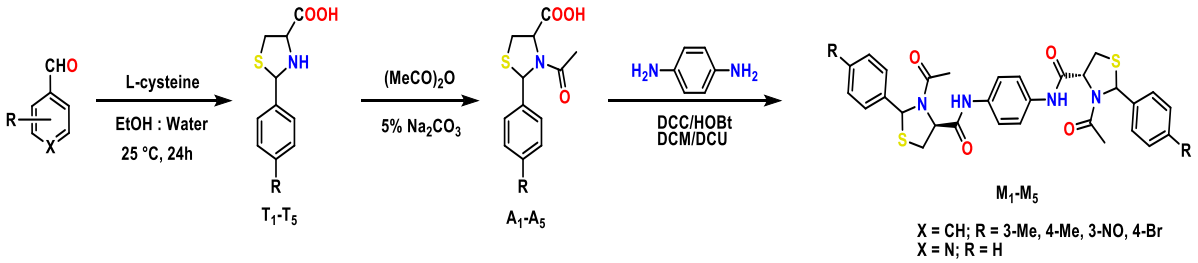

Scheme 1. Prepare of bis thiazolidine amide derivatives.

of Basrah, Iraq and University of Tehran, Iran. Human cancer cell lines (PC-3) were provided and cultured in Dulbecco's modified Eagle's medium (DMEM) with 1% penicillin–streptomycin and 10% fetal bovine serum (FBS) (Gibco) in a humidified environment with 5% CO_2 at 37 °C (Model Wave XS2, BioTek, USA). The materials were purchased from WuXi AppTec. Absorption spectrophotometry was analyzed at 570 nm on a flow cytometer apparatus, Partec PAS, Germany.

2.2. Preparation of Thiazolidine cycle [T1-T5]

20 mmole of aldehyde derivatives in a round bottom flask with 20 mmole of L-cysteine were mixed in 100 ML of ethyl alcohol and 10ML of water. The mixture was stirred for 24 hours at 25 °C, resulting in a white precipitate, which was filtered, washed with diethylether, dried, and recrystallized using a mixture of ethanol and water. The obtained products are presented in Scheme 1. These products are a mixture of diastereomers, *cis* (2*R*,4*R*), and *trans* (2*S*,4*R*) [21,41].

2.3. Preparation of 3-acetyl thiazolidine [A1-A5]

A mixture of 20 mmoles of compounds [T1-T5] was dissolved in a solution containing 50 ML of 5% sodium carbonate in an ice bath, followed by the addition of 3.6 ML of acetic anhydride. The solution was then left stirring for 1.5 h. Afterward, the mixture was acidified and extracted with ethyl acetate. Organic layer was washed with water and evaporated, resulting in a white precipitate. Crystallization was performed using a mixture of ethyl alcohol and water. The mixture was then analyzed by thin-layer chromatography (TLC) using an eluent of ethyl acetate and hexane (7:3) [41].

(2S, R / 4R) 3-acetyl-2-m-tolylthiazolidine-4-carboxylic acid (A2)

White Crystall, Yield: 85%, m.p: 161–164°C. FT-IR (KBr, cm^{-1}): 3350s (OH), 3010w (C-HAr), 2980w (C-Halph.), and 1732s (C = O). ^{1}H-NMR (400 MHz, δ; ppm, *J*; Hz) δ 1.55s (3H, CH_3), δ 1.8s (3H, CH_3), δ 3.28 m, 3.55 t (2H, H5), 4.45 m (1H, H4), δ 6.52s (1H, H2), δ 7.1-7.7 m (4H, H-Ar), and δ 11.95 s (1H, OH).

(2S, R / 4R) 3-acetyl-2-(4-methyl-3-nitrophenyl) thiazolidine-4-carboxylic acid (A3)

White powder, Yield: 82%, m.p: 172–174°C. FT-IR (cm^{-1}): 3380s (OH), 3060w (C-HAr), 2988w (C-Halph.), and 1728s (C = O). ^{1}H-NMR (400 MHz, δ; ppm, *J*; Hz) δ 1.6s (3H, CH_3), δ 1.82 s (3H, CH_3), δ 3.2, 3.56 m (2H, H5), 4.43 m (1H, H4), δ 6.34 s (1H, H2), δ 7.15-7.8 m (3H, H-Ar), and δ 12.1s (1H, OH).

(2S, R/4R) 3-acetyl-2-(pyridin-4-yl) thiazolidine-4-carboxylic acid (A5)

White powder, Yield: 70%, FT-IR (cm^{-1}): 3350 m (OH), 3050w (C-HAr), 2928w (C-Halph.), and 1735s (C = O). ^{1}H-NMR (400 MHz, δ; ppm, *J*; Hz) δ *trans* (2S, 4R) major isomer (ratio 80: 20): δ 1.81s (3H, CH_3), δ 3.2 m, 3.65 t (2H, H5), 4.5 m (1H, H4), δ 6.55 s (1H, H2), δ 7-7.6d (4H, H-Ar), and δ 12.08 s (1H, OH).

2.4. Synthesis of bis thiazolidine amide derivatives [M1-M5]

A mixture of 0.002 moles of compounds A1-A5, 0.002moles of N,N'-Dicyclohexylcarbodiimide (DCC), and 0.002 moles of 1-Hydroxybenzotriazole (HOBt) in dichloromethane. The solution was stirred at 0 °C for 10

min., followed by adding 0.001 moles of 1,4-phenylenediamine to the solution. The mixture was continuously stirred for 24 h at 25 °C, forming a white solid compound. The solution was filtered, and the white solid was collected, identified as DCU (Dicyclohexylurea). The filtrate reaction was diluted with 30 ML of CH_2Cl_2, washed with a 5% $NaHCO_3$ solution, followed by a 10% citric acid solution, then NaCl (solution brain), and finally distilled water. A mixture was dried by adding Na_2SO_4, filtered, and the evaporated to form a precipitate, which was recrystallized using a mixture of hexane and chloroform (3:1). The chemical apparatus was evaluated with TLC using a solvent mixture of tetrahydrofuran, benzene, and formic acid (2:6:2). This resulted in a mixture of diastereomers, *cis* (2*R*,4*R*), and *trans* (2*S*,4*R*) [41].

(2S, R/4R)-N, N'-(1,4-phenylene) bis(3-acetyl-2-phenylthiazolidine-4-carboxamide) (M1)

Yellow crystals, Yield: 27%, m.p:122-124 °C, Rf = 0.44. FT-IR Spectrum (KBr, cm^{-1}): 3375w (NH str.), 3050 w (CH-Ar), 2933w (CH-aliphatic), 1730m, 1680s (C = O amide), 1618 m (NH bend) and 1608 m (NH bend). ^{1}H-NMR (400 MHz, δ; ppm, *J*; Hz); show the four diastereomers (Scheme 1). *trans* isomer (2*S*, 4*R*) Major; δ 1.86s (6H, 2 CH_3), δ 3.09 m (2H, *J* = 8.00 Hz, H5), δ 3.40 m (2H, *J* = 8 Hz, H5), δ 4.68 m (2H, *J* = 8.00 Hz, H4), δ 6.47s (2H, H2), δ 7.24-8.1 m (14H, H-Ar), δ 9.85 s (br, 2H, NH). ^{13}C-NMR (100 MHz, DMSO-d_6, δ, ppm) δ 23.05 (CH_3), 32.3 (C5), 64.8(C4), 66.6 (C2), 114–146 (CAr), 168.3, 169 (C = O amide). Mass spectra EI. (70 ev); m/z: 574 [$M^{\cdot+}$], the base peak 121 and the fragments: 43, 164, 219, and 425. The Mass spectra, FT-IR, ^{1}HNMR, and ^{13}CNMR data were presented in supplementary file as figures S1-4, respectively.

(2S, R/4R)- N,N'(1,4-phenylene) bis(3-acetyl-2-m-tolylthiazolidine-4-carboxamide) (M2)

Yellow powder, Yield: 26%, m.p:140-142 °C, Rf = 0.38. FT-IR Spectrum (KBr, cm^{-1}): 3265 m (NH str.), 3059w (CH-Ar), 2933w (CH-aliphatic), 1714m, 1670s (C = O amide), and 1595 m (NH bend). ^{1}H-NMR (400 MHz, δ; ppm, *J*; Hz); show the four diastereomers, *trans* isomer (2*S*, 4*R*) major; δ 1.64 s (6H, $2CH_3$ Ar), δ 1.88 s (6H, $2CH_3$), δ 3.36 m (2H, *J* = 8.00 Hz, H5), δ 3.42 m (2H, *J* = 8.00 Hz, H5), 4.7 m (2H, *J* = 8.00 Hz, H4), δ 6.58 s (2H, H2), δ 6.98-7.82 m (12H, H-Ar), and δ 10.64s (br., 2H, NH). ^{13}C-NMR (100 MHz, DMSO-d_6, δ, ppm) δ 15.11(CH_3– Ar), 20.8 (CH_3), 33.7 (C5), 62.8(C4), 67(C2), 117–147 (CAr), 167.9, 172 (C = O amide). Mass spectra EI. (70 ev); m/z: 602 [$M^{\cdot+}$], the base peak 185, and the fragments: 43, 77, 105, and 306. The mass spectra, FT-IR, ^{1}HNMR, and ^{13}CNMR are presented in supplementary file as figures S5-8, respectively.

(2S, R/4R) N,N' (1,4-phenylene) bis(3-acetyl-2-(3-nitrophenyl) thiazolidine-4-carboxamide) (M3)

Yellow, dark crystals, Yield: 20%, m.p:130-132 °C, Rf = 0.57. FT-IR Spectrum (KBr, cm^{-1}): 3199w (NH str), 3064w (CH-Ar), 2929w (CH-aliphatic), 1739m, 1707s (C = O amide), 1608 m (NH bend), 1550 m, and 1390 (NO_2). ^{1}H-NMR (400 MHz, δ; ppm, *J*; Hz); show the four diastereomers, trans isomer (2*S*, 4*R*) major; δ 1.61s (6H, $2CH_3$ Ar), δ 1.90 s (6H, $2CH_3$), δ 3.09 m (2H, *J* = 8.00 Hz, H5), δ 3.47 m (2H, *J* = 8.00 Hz, H5), 4.7 m (2H, *J* = 8.00 Hz, H4), δ 6.52s (2H, H2), δ 7.1-8.05 m (10H, H-Ar), and δ 10.04s (br., 2H, NH). ^{13}C-NMR (100 MHz, DMSO-d_6, δ, ppm) δ 16.2(CH_3 Ar), 24.8 (CH_3), 32.7(C5), 64.8(C4), 67.2(C2), 115–149 (CAr), 171, 173.2 (C = O amide). Mass spectra EI. (70 ev); m/z: 692 [$M^{\cdot+}$], the base peak 135 and the fragments: 43, 77, 107, 161, and 426. The mass spectra, FT-IR, ^{1}HNMR, and ^{13}CNMR data are provided in supplementary file as figures S9-12, respectively.

(2S, R/4R)- N, N'-(1,4-phenylene) bis(3-acetyl-2-(4-bromophenyl) thiazolidine-4-carboxamide) (M4)

Dark beige crystals, Yield: 28%, m.p: 160–163 °C, Rf = 0.44. FT-IR Spectrum (KBr, cm^{-1}): 3111w (NH str.), 3080w (CH-Ar), 2920w (CH-aliphatic), 1734m, 1700s (C = O amide), and 1627 m (NH bend). ^{1}H-NMR (400 MHz, δ; ppm, *J*; Hz); show the four diastereomers, *trans isomer* (2*S*, 4*R*) Major; δ 1.86s (6H, $2CH_3$), δ 3.11 m (2H, *J* = 8.00 Hz, H5), δ 3.47, m (2H, *J* = 8.00 Hz, H5), δ 4.71 m (2H, *J* = 8.00 Hz, H4), δ 6.43s (2H, H2), δ 7.33-8.17d (12H, H-Ar), and δ 10.31s (br., 2H, NH). ^{13}C-NMR (100 MHz, DMSO-d_6, δ, ppm) δ 23 (CH_3), 32.4,(C5) 64.9(C4), 66.7(C2), 120–146 (CAr), 169.3, and 172.4 (C = O amide). Mass spectra EI. (70 ev); m/z: 732 [$M^{\cdot+}$], the base peak 145, and the fragments: 43, 71, 294, and 426. The Mass spectra, FT-IR, ^{1}HNMR, and ^{13}CNMRdata are presented in the supplementary file as figures S13-16, respectively.

(2S, R/4R)- N, N' (1,4-phenylene) bis(3-acetyl-2-(pyridin-4-yl) thiazolidine-4-carboxamide) (M5)

Beige dark powder, Yield: 24%, m.p:151-153°C, Rf = 0.3. FT-IR Spectrum (KBr, cm^{-1}): 3240 m (NH str.), 3028w (CH-Ar), 2962w (CH-aliphatic), 1722m, 1680s (C = O amide), 1600 m (NH bend), and 1640 m (C = N). ^{1}H-NMR (400 MHz, δ; ppm, *J*; Hz); show the four diastereomers, *trans* isomer (2*S*, 4*R*) Major; δ 1.85s (6H, $2CH_3$), δ 3.07,

m (2H, J = 8.00 Hz, H5), δ 3.44 m (2H, J = 8.00 Hz, H5), δ 4.67 m (2H, J = 8.00 Hz, H4), δ 6.44, s (2H, H2), δ 7.12-8.17d (12H, H-Ar), and δ 10.02s (br., 2H, NH). ^{13}C-NMR (100 MHz, DMSO-d_6, δ, ppm) 20.5 (CH_3), 36.6 (C5), 55.6, 60.6(C4,C2), 110–156 (CAr), 168.5, and 172.6 (C = O amide). Mass spectra EI. (70 ev); m/z: 576 [M^{-+}], the base peak 233 and the fragments: 43, 79, 136, 206, and 426. The Mass spectra, FT-IR, ^{1}HNMR, and ^{13}CNMR data are provided in the supplementary file as figures S17-19, respectively.

2.5. Molecular docking studies

All docking processes were conducted using Schrodinger's Maestro software. The details of a docking process are reported in a supplementary file. Briefly, both proteins, Androgen Receptor Ligand-binding Domain W741L Mutant (PDB ID: 1Z95) and epidermal growth factor receptor tyrosine kinase domain (PDB ID: 1M17), were retrieved from the protein data bank and were imported into Maestro. The heteroatoms were removed along with water, and the protein was prepared using the default setting. The ligands were imported as SMILEs into Maestro and prepared using the LigPrep panel using the default setting, and all stereoisomers were generated. All docking processes were conducted using an OPLS3 force field.

2.6. ADME analysis

The pharmacokinetic properties (ADME), along with characteristics such as blood–brain barrier (BBB) penetration, Pg protein affinity, and bioavailability, were estimated using SwissADME [49]. The molecular structures of a newly prepared compound (M1-M5) were created using ChemDraw. The prediction process was launched once these structures were assigned labels using the SMILES (Simple Molecular Input Line Entry System), with the results presented in Table 2.

2.7 Molecular dynamics simulations study

Molecular dynamics (MD) simulations were performed using GROMACS (version 2022) with the CHARMM36 force field. The system, consisting of a protein–ligand complex, was solvated in a cubic simulation box with a 10 Å buffer using the TIP3P water model, and neutralized with counterions (Na^+/Cl^-). Energy minimization was conducted using the steepest descent algorithm until the maximum force fell below 200 kJ/mol/nm. Equilibration involved NVT (1 ns) at 300 K with the V-rescale thermostat and NPT (1 ns) at 1 atm using the Parrinello-Rahman barostat. A 100 ns production MD simulation was performed under NPT conditions with a 2 fs time step, PME method for electrostatics, and LINCS constraints for bond lengths. Structural stability and flexibility were assessed using root mean square deviation (RMSD) and root mean square fluctuation (RMSF) analyses [50]. Principal Component Analysis (PCA) was applied to analyze essential motions by aligning the trajectory and extracting backbone atom coordinates via MDAnalysis (Python library), followed by PCA using scikit-learn, with results visualized in a PCA scatter plot. MM-GBSA calculations were performed in Prime (Schrödinger Suite) after molecular docking to evaluate ligand binding energy using the OPLS4 force field. All simulations were conducted on an NVIDIA GPU-equipped workstation using GROMACS, Schrödinger's Maestro, Prime for MM-GBSA, MD analysis, and Matplotlib for visualization [51].

2.7. Antibacterial Activity

The synthesized compounds (M1-M5) were studied against three strains of bacteria *S. aureus* (*Staphylococcus aureus*), *E. coli* (*Escherichia coli*), and *S. mutans* (*Streptococcus mutans*) using broth microdilution techniques to determine their least inhibitory concentrations (MICs) according to the Clinical Laboratory Standard Institute (CLSI) guidelines. The MIC was defined as the lowermost concentration of each compound (M1-M5) required to inhibit the visible growth of the tested bacteria. Two-fold consecutive dilutions of all compounds (M1-M5) were prepared in a concentration range of 5000-9.7 µg/ML in germ-free plastic micro-dilution trays containing Mueller Hinton broth. Bacterial inoculate of each strain were prepared from freshly cultured cells in sterile normal saline adjusted to a 0.5 McFarland standard. These suspensions were further diluted (1:100) with germ-free Mueller-Hinton broth (MHB) just before addition to the trays containing serial dilutions of all

compounds (M1-M5), resulting in a final concentration of approximately 1 × 105 CFU/ML bacterial cells for each compound. The 96-well plates were then incubated at 37°C for 24 h, and the development pointer resazurin was used. Briefly, 4 µl of a 4 mg/ML stock solution of resazurin in germ-free water was added to all wells. Pink coloration indicated bacterial growth in the wells. The least bactericidal concentration was recorded as the lowest concentration of each compound (M1-M5) that could kill 99.99% of the tested bacterial cells. For the determination of minimum bactericidal concentrations (MBCs), 100 µl of the contents of wells showing no growth in the MIC experiment were cultured on Nutrient agar plates and incubated for 24 hours at 37°C before recording MBC values [41].

2.8. MTT Activity

The effect of the synthesized compounds (M1-M5) on prostate cancer (PC3) cells was studied. Human prostate cancer cells (PC3) were obtained from the National Cells Banks in Iran. Following a well-established method, the prostate cancer cells were cultured in 96-well plates and incubated at 37°C for 72 h. Subsequently, a series of concentrations of the prepared compounds (M1-M5) was prepared using DMSO as a solvent and added to each well. The effectiveness of the prepared compounds was determined by measuring absorbance at a wavelength of 570 nm. The concentrations of compounds (M1-M5) resulting in half-cell death were determined, and the IC_{50} values were obtained from the dose–response curve.

2.9. Apoptosis and Cell Cycle Analysis

The compound M4 was studied against prostate cancer cells (PC3) to assess the acridine test, apoptosis, and cell cycle. Identification of apoptotic and necrotic prostate cancer cells (PC3) treated with compound M4 was achieved using Annexin V-FITC apoptosis kit from (BioVision). Afterward, treating cells for 24 hours with the IC_{50} concentration of M4, the cells were gathered, methodically washed, and processed with propidium iodide (PI) and fluorescein isothiocyanate (FITC) according to a manufacturer's protocol. Briefly, 5×10^5 cells were treated with M4 at the IC_{50} concentration for 24 h, and untreated control cells were harvested and centrifuged. The pellet was then resuspended in 500 µl of binding buffer, and 5 µl of annexin V-FITC and 5 µl (50 µg/ML) of propidium iodide were added before incubation at 25°C for 5 min. After incubation, the stained cells were analyzed using flow cytometry (flow cytometer apparatus, Partec PAS, Germany). Differentially labeled cells were identified by acquiring signals from annexin V-FITC-labeled cells via the FITC signal detector (FL1) and PI-stained cells via the FL2 signal detector.

3. Result and Discussion

3.1. Synthesis of (M1-M5) compounds

The *N,N′* (1,4-phenylene) Bis(3-acetyl-2-phenylthiazolidine) substituted-4-carboxamide derivatives (M1-M5) were prepared in a multiple-step reaction. Firstly, the aromatic aldehyde reacted with L-cysteine to produce a thiazolidine-4-carboxylic acid (T_1-T_5) in good yield. Secondly, the amino group of the thiazolidine ring (T_1-T_5) was acylated using acetic anhydride to produce 3-acetylthiazolidine-4-carboxylic acid derivatives (A_1-A_5). Finally, the derivatives bis amide thiazolidine (M_1-M_5) were prepared by reacting 1,4-phenylenediamine with compounds (A1-A5) in a ratio of (1:2) in the presence of catalysts DCC (*N,N*-dicyclohexyl carbodiimide) and HOBt. The obtained product *N,N′*-(1,4-phenylene) bis (3-acetyl-2-phenylthiazolidine substituted-4-carboxamide) was characterized using spectroscopic techniques [41], as shown in Scheme 1 and the mechanism bis amide thiazolidine shown in Scheme 2.

It is worth mentioning that the thiazolidine cycle consists of a mixture of diastereomers known optical isomer. These include trans diastereomers (C2 – (2S, 4R)) and cis diastereomers (C2 – (2R, 4R)), The ratio of *cis* and *trans* isomers depends on a nature of the solvent used, with the *trans* isomer being predominant in DMSO solvent (trans >50) and the *cis* diastereomers being dominant in $CDCl_3$ (cis > 50), Scheme 3.

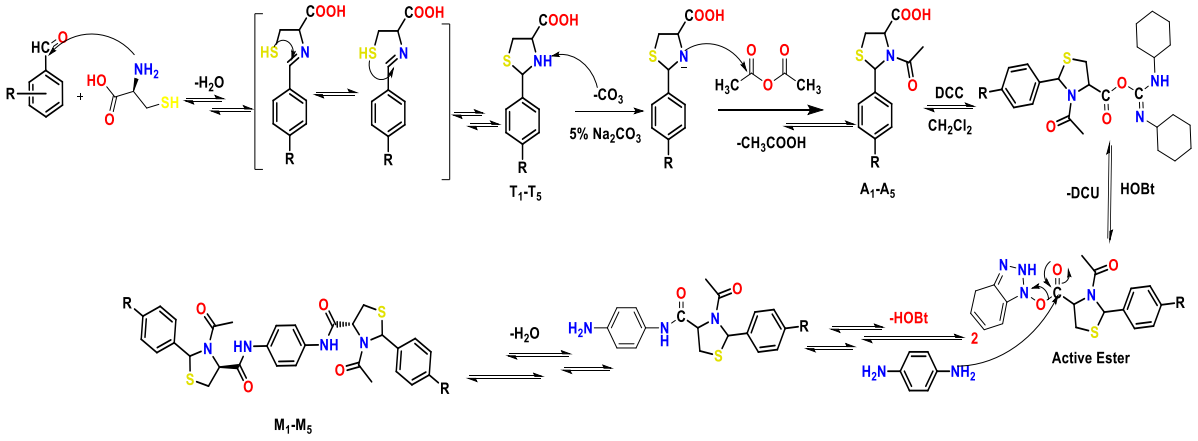

Scheme 2. Mechanism of prepare bis thiazolidine amide derivatives.

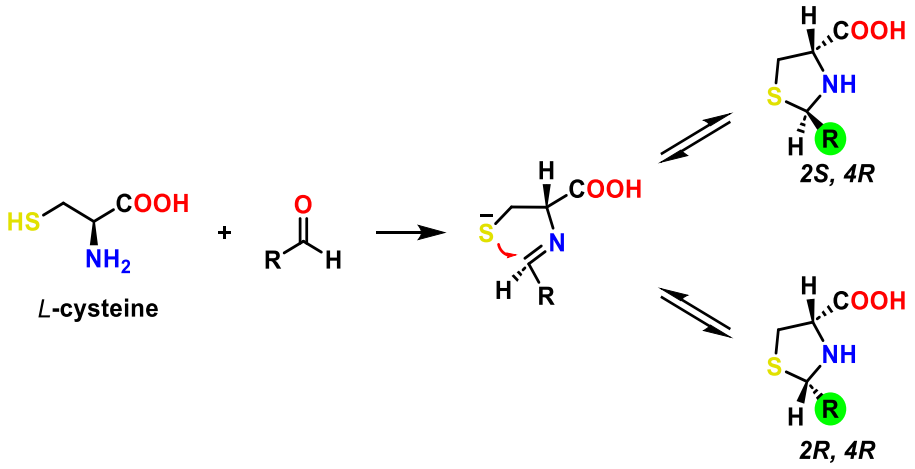

Scheme 3. The thiazolidine isomers mixture formation.

3.2. Molecular docking studies of Bis amide thiazolidine

The obtained compounds were docked against both Androgen Receptor (AR) Ligand-binding Domain W741L Mutant (PDB ID: 1Z95) and epidermal growth factor receptor – tyrosine kinase domain (PDB ID: 1M17) to study their possible interactions; hence, their mechanism of action.

Regarding the AR protein, it was found that these compounds could not fit inside the active site of the domain due to their size, which indicates that these compounds may have mechanisms of action different from the inhibition of AR protein. An attempt was made to force the compounds inside the active site using MOE software, and it was found that the docking scores were highly unfavored with positive values.

Table 1. Docking score of the bis amide thiazolidine derivatives inside the active site of EFGR.

Compound	Docking score (kcal/mol)	Residue/interaction type	Distance (Å)
M5	−6.717	Lys692/H-bond	1.84
		Pro770/H-bond	2.09
M1	−6.547	Lys721/π-cation	5.03
M3	−6.259	Lys692/H-bond	1.81
		Cys773/H-bond	2.28
M4	−6.129	Lys721/π-cation	5.20
M2	−5.607	Lys692/H-bond	1.71
Gefitinib	−6.212	Lys721/H-bond	2.79
		Asp831/π-cation	4.72

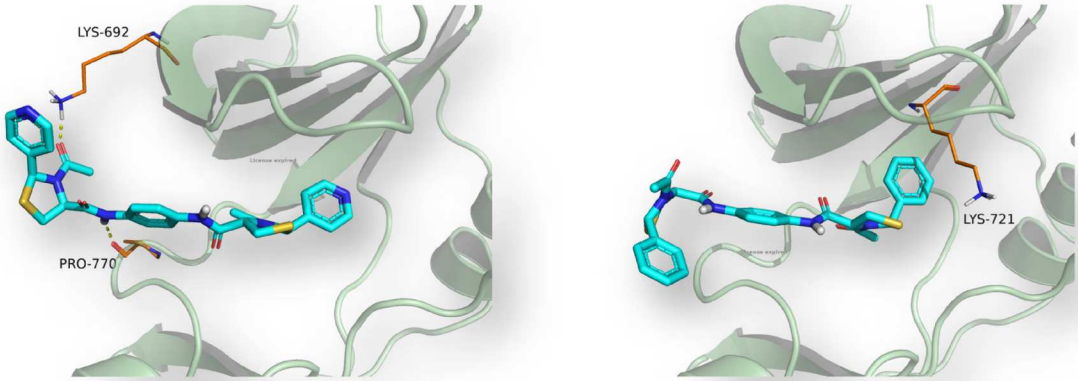

Figure 4. Interaction of compound M5 (left) and M1 (right) with the active site of the EGFR.

Next, the possibility of these compounds to inhibit tyrosine kinase was investigated by targeting the EGFR (epidermal growth factor receptor). Compounds $M_{1\text{-}5}$ were docked into the active site of the EGFR, and the results obtained are listed in Table 1.

The focus was on EGFR inhibition due to its pivotal role in cancer progression and drug resistance. The docking studies revealed strong binding affinities between the compounds and EGFR, suggesting that inhibition of this receptor, rather than the androgen receptor, underlies their anticancer effects. The rationale for targeting EGFR stems from its overexpression in prostate cancer, where it promotes tumor growth and survival. Compound M4 emerged as the most promising candidate, exhibiting stable binding interactions, which correlated with its high biological activity.

As seen in Table 1, compounds M5, M1, and M3 showed a docking score higher than the reference drug Gefitinib. M5 showed a docking score of – 6.717 kcal/mol and formed two H-bonds toward Lys692 and 770 with 1,84 and 2.09 Å, respectively. On the other hand, compound M1 was able to form π-cation interaction toward Lys721, which resulted in a docking score of – 6.547 kcal/mol, indicating that vdW interactions play a significant role in the interactions of these compounds. M3 also showed a superior docking score (−6.259 kcal/mol) and formed two hydrogen bonds with residues Lys692 and Cys773. The interactions of compounds M5 and M6 are shown in Figure 4.

Gefitinib forms a hydrogen bond with Lys721 at 2.79 Å, while M4 forms a stronger hydrogen bond with Lys692 at 1.71 Å. Additionally, Gefitinib interacts with Asp831 through a stabilizing π-cation interaction at 4.72 Å, whereas M4 interacts with Lys721 at a slightly longer distance of 5.20 Å. The shorter distance of M4's hydrogen bond suggests a stronger interaction with Lys692, while the longer distance for M4's π-cation interaction indicates a potentially weaker binding compared to the one formed by Gefitinib with Asp831.

3.3 ADME studies

The pharmacokinetic properties (ADME) and other characteristics, such as (BBB) blood–brain barrier penetration, P-glycoprotein (Pg) affinity, and bioavailability were evaluated using Swiss-ADME. The molecular structures of newly prepared compounds (M1-M5) were constructed using ChemDraw. Once labeled with the SMILES, the prediction process was initiated, and the results were obtained in Table 2. Swiss-ADME

Table 2. ADME studies of compounds (M1-M5).

COMP	nRB	nHBA	nHBD	TBSA (A°)	BS	Logs	GI	BBB	Pgp	iLOGP	Ro5
M1	10	4	2	149.42	0.55	−6.32	low	No	Yes	3.16	Yes
M2	10	4	2	149.42	0.55	−7.08	low	No	Yes	3.55	Yes
M3	12	8	2	241.06	0.17	−7.89	low	No	Yes	2.55	No
M4	10	4	2	149.42	0.55	−7.75	low	No	Yes	4.32	Yes
M5	10	6	2	175.2	0.55	−4.64	low	No	Yes	2.84	Yes

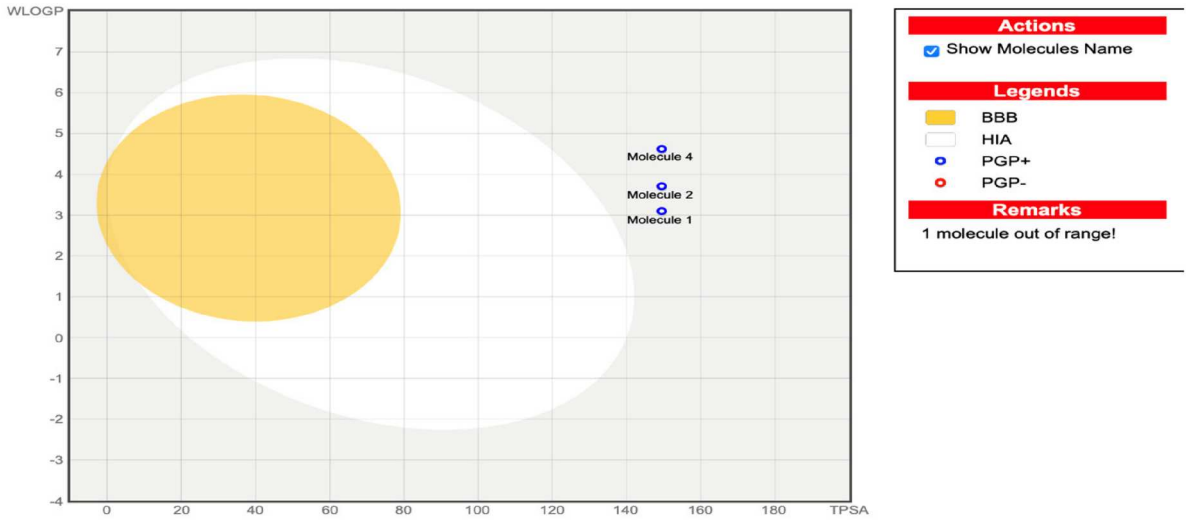

Figure 5. The boiled egg model for compounds [M1-M4] shows GIT-absorbable molecules in the white region and brain-permeable molecules in the yellow yolk region where one compound M3 out of the range and all molecules have low absorption and do not penetrate BBB.

was employed to assess the pharmacokinetic profile of the drugs (M1-M5), including their absorption, distribution, metabolism, and excretion (ADME) [51]. BBB penetrating, bioavailability and Pg affinity. Various parameters such as nHBA, nRB, nHBD, TBSA, BS, gastrointestinal (GI) absorption, BBB penetration, Pgp binding, iLOGP, and parentage human oral absorption were determined. Additionally, Lipinski's of five were calculated to evaluate drug likeness. Table 2 outlines the ADME-related properties and drug likeness characteristics. Topological polar surface area (TPSA), which influences drug bioavailability by affecting gastrointestinal absorption and BBB penetration, was also analyzed. According to Clark (2011), compounds with TPSAs exceeding 140 A° have reduced oral bioavailability. Compounds M1, M2 and M4exhibited a TBSA of 149 A° while compound M5 had a TPSA of 175.2 A°. In contrast, compound M3 showed a higher TPSA of 241.42 A° with a bioavailability score of 0.17, whereas the remaining compounds had a bioavailability score of 0.55. None of the compounds was able to cross the BBB, and all were found to bind to P-glycoprotein (Pgp), a protein that hinders cellular drug uptake and utilization. Furthermore, all compounds violated Lipinski's Rule of Five except for compound M3.

The Swiss ADME webserver developed the brain or Intestinal Estimated Permeation (BOILED-EGG) model and the Egan egg graph for novel chemicals. This model predicts brain and intestinal absorption, allowing intuitive assessment of passive GIT absorption and brain penetration (BBB) based on molecule positioning in WLOGP-TPSA space. Figure 5 demonstrates that all chemicals can be inertly absorbed from GIT (white area) but cannot penetrate the brain (yolk). Pgp (PGP+) is predicted to actively efflux all of them.

3.4 MD simulation

Given the prominence of theoretical studies on conformational stability, it is worthwhile to examine the influence of compounds on targeted proteins using MD simulations [(51)]. Over 100 ns, we studied the conformational behavior of the EGFR protein in complex with compounds M3 and M4. We analyzed the impact of these compounds on the structural integrity of EGFR residues over time using the RMSD of the protein backbone. The data generated from the MD simulations provided adequate structural insights into chemical variations in configurations and ligand – protein interactions. The MD simulations for the compounds were carried out based on the docking results. Structural modifications were analyzed using Root Mean Square Deviation (RMSD) plots from the MD trajectory. RMSD plot exhibited a stable association between M4 and EGFR protein, with a ligand RMSD fluctuations residual approximately 2.0 A° and the protein remaining within approximately 3.2 A°. compound M4 showed high binding capacity, though M3 exhibited a slight unstable interaction capacity. The EGFR-M4 complex remained constant during the MD simulation (Figure 6). The EGFR-M4 complex displayed a strong binding relationship throughout MD simulation.

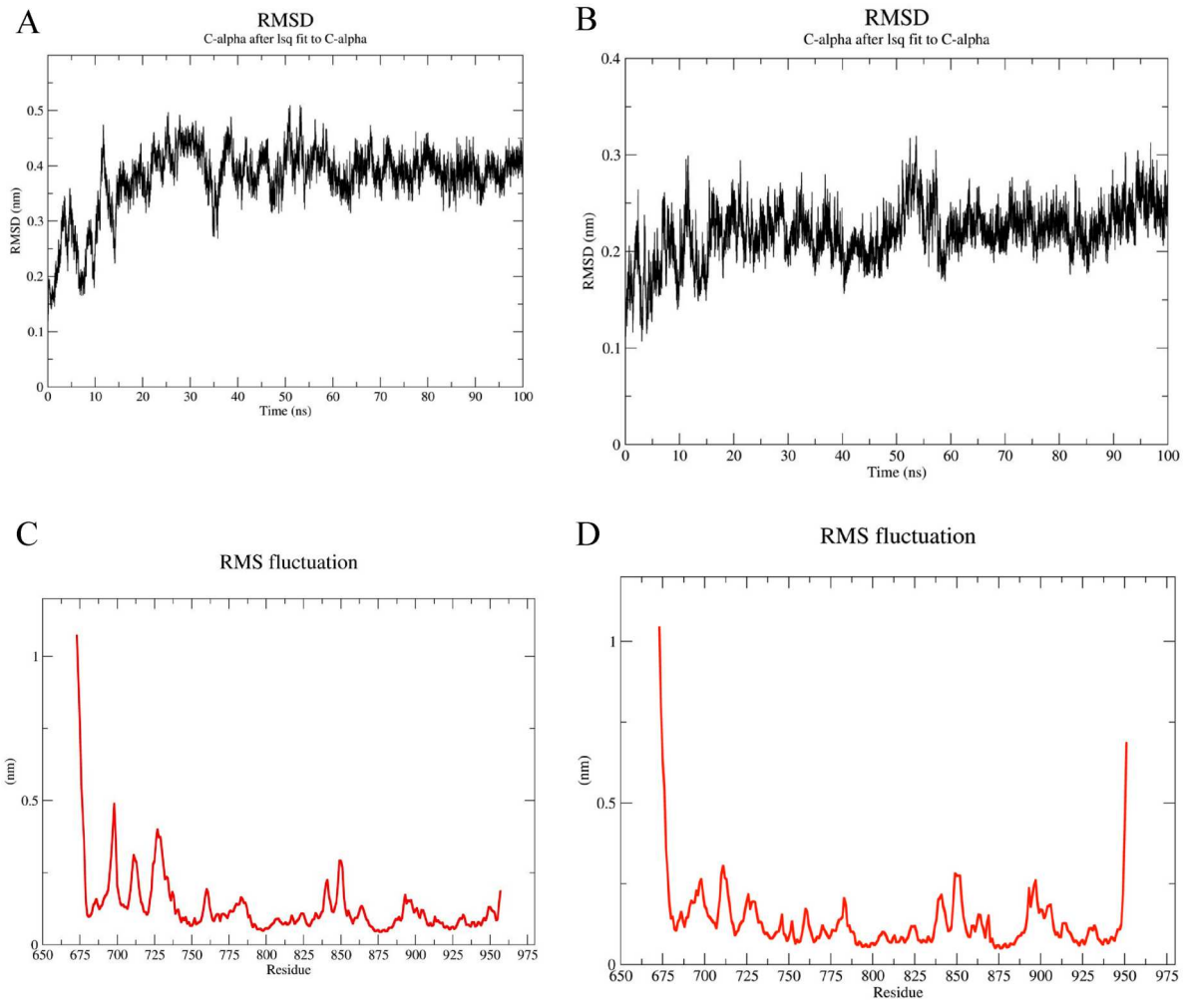

Figure 6. RMSD plot (A) M3 compound and (B) M4 and RMSF plot (C) M3 and (D) M4.

After the initial rise, the RMSD fluctuates around 0.3–0.5 nm. This suggests the structure reached as table state with dynamic flexibility but no major conformational changes.

3.5 Principal component analysis (PCA)

The essential dynamic method serves as a powerful tool for exploring the dynamical behavior of the EGFR protein in combination with M3 and M4 the analysis is complicated, comparing drug bound and drug unbound forms of the EGFR as reference. A gain deeper insight into the configurational two principal components (PC1 and PC2) was selected to project the trajectories during the simulations of both ligand-free and ligand bound EGFR as shown in Figure 7(A, B). The simulation results revealed that the unbound EGFR explored a broader region of the phase space whereas drug bound systems occupied more confined regions. Among the compounds, M4 demonstrated the most significant reduction in essential dynamic motions, indicating a stronger effect on protein flexibility compared to M3. Furthermore, the PCA results suggest that drug bound EGFR exhibits greater stability than its ligand-free counterpart. These findings align well with the RMSD and RMSF analyses strengthening of a study's conclusion.

3.4. Biological activity

3.4.1. Antibacterial Activity

All amide thiazolidine compounds (M1-M5) showed promising biological activity against three strains of bacteria (*S. aureus, E. coli, and S. mutans*). The minimum inhibitory concentration (MIC), minimum bactericidal

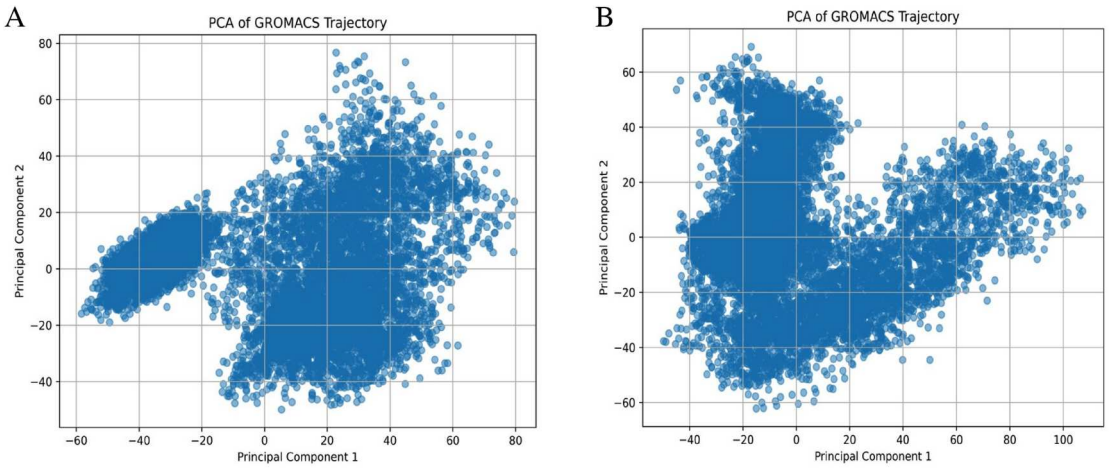

Figure 7. Two-dimensional projection of motion of trajectory of EGFR bound with A (M4) and B (M3).

Table 3. Biological activity of (M1-M5) compounds against various kinds of bacteria (*S. aureus*, *E. coli*, and *S. mutans*) relative to that of cefixime.

	S. aureus			*E. Coli*			*S. mutans*		
Sym.	In hib. of 10000 ppm	MIC ppm	MBC	In hib. of 10000 ppm	MIC ppm	MBC	In hib. of 10000 ppm	MIC ppm	MBC
M1	16 mm	312	625	10 mm	1250	1250	20 mm	625	1250
M2	19 mm	156	312	13 mm	625	1250<	19 mm	312	625
M3	20 mm	79	79	4 mm	1250<	1250<	22 mm	79	312
M4	28 mm	9.7	9.7	10 mm	1250<	1250<	22 mm	312	312
M5	26 mm	39	79	0 mm	1250<	1250<	23 mm	79	156
Cefixime	15 mm	312	625	4 mm	1250<	1250<	19 mm	156	312

concentration (MBC), and inhibition zone were calculated at a concentration of 10,000 ppm, as shown in Table 3. Compounds M4 and M3 displayed good activity against bacteria *S. aurous*, with MIC values of 9.7 and 79 ppm, respectively. Additionally, the relationship between the structure compound and the cellular tissues of bacteria was studied. These compounds contain active groups (Br, NO_2) with electronic doublets, which can inhibit bacteria, along with the effectiveness of the amide group and the thiazolidine ring. Compound M4 exhibited the highest effectiveness and activity in killing bacteria *S. aureus*, penetrating their internal membranes, and destroying them. The results were compared with those of a well-known antibiotic (Cefixime), confirming its effectiveness [46].

3.4.2. Anti-prostate cancer cell activity

The anticancer activity against prostate cancer type PC3 was examined for all newly prepared compounds (M1-M5). The inhibition effectiveness against cancer cells was measured at six concentrations (100, 50, 25, 12.5, and 6.25 µg/ML), and the half-inhibitory concentration (IC_{50}) value was calculated graphically and mathematically, as shown in Table 4.

All compounds exhibited high effectiveness against PC3 cancer cells. Compound M4 was the most effective among the prepared compounds, with a significant inhibition rate and an IC_{50} value of 19.56

Table 4. MTT study of (M1-M5) compounds using PC3 (human prostate cancer) cell lines.

Compound	IC_{50} (Anti-cancer µg/ML)					
	Inhibition 100 µg/ML	Inhibition 50 µg/ML	Inhibition 25 µg/ML	Inhibition 12.5 µg/ML	Inhibition 6.25 µg/ML	IC_{50} µg/ML
M1	26.03	57.44	72.52	82.85	97.62	50.86 ± 0.95
M2	20.87	55.86	80.48	90.81	97.11	50.40 ± 0.9
M3	19.63	39.15	71.82	81.30	88.55	36.87 ± 0.94
M4	12.00	26.93	47.06	66.53	69.97	19.56 ± 0.97
M5	18.29	23.76	65.39	78.93	93.39	30.55 ± 0.95
Darolutamide	22.83	56.54	79.79	88.85	97.85	52.82 ± 0.90

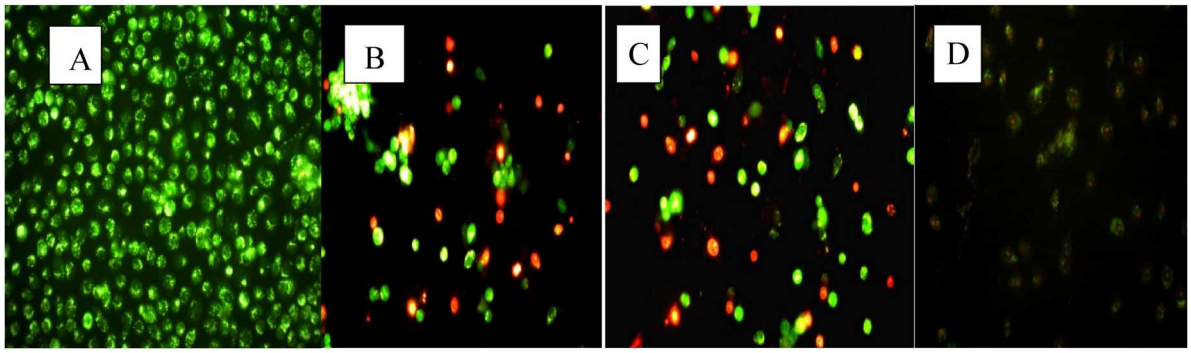

Figure 8. (A) Untreated cancer cells (Control), (B) and (C) Cancer cells treated with compound M4 showing penetration of the compound into membranes, and (D) Death of cancer cells observed after some time.

µg/ML. This effectiveness is attributed to the presence of the thiazolidine ring, as well as the replacement of the H group with a Br group, which enhanced effectiveness due to the bromine group's electron-withdrawing ability and its participation in electron doublets, as well as binding to cancer cell proteins. The relationship between the composition, binding sites, and the interaction between the prepared compounds and cancer cell proteins was studied, suggesting the potential future use of these compounds as treatments against cancer cells. The active compound M4 was treated with acridine/ethidium bromide (EB/AO), aiming to elucidate its effect on the plasma membrane of cancer cells and to observe any changes in cancer cell membranes indicative of programed cell death. The cells were treated with half of the inhibitory concentration (IC_{50}) of compound M4. It was observed that live cancer cells exhibited a change in shape, appearing in green and red-orange due to the compound's effect, which led to the destruction of the plasma membrane and subsequent illumination in orange. This also indicated their interaction with the cells' DNA and its consequent effect [21]. The cells displayed signs of necrosis and programed cell death, as depicted in Figure 8. The efficacy results of the compounds against PC3 cancer cells are presented in the supplementary file as figures 20, 21 and 22.

3.4.3. Apoptosis assay of amide M4

Apoptosis is the mechanism of eliminating unwanted cells in living tissues and is considered one of the effective strategies for killing cancer cells. Apoptosis is linked to the cell's plasma membrane through its effect on cell shape, chromatin cohesion, cell shrinkage, and loss of living organelles in the cytoplasm. The bis amide thiazolidine derivative M4 was selected to evaluate its ability to induce cell death, its effect on programed cell death due to its distinctive and effective structure, and its containment of more than one group that could bind with the protein (Figure 9). The cancer cells were cultured and stored for 48–72 h and the seized with a colored substance to clarify them, and the morphological changes of the cells were observed according to the IC_{50} concentration. Analysis and flow cytometry were conducted by double annexin-FITC staining, revealing an increase in apoptosis of PC3 cells (live cells Q4, dead cells Q1,

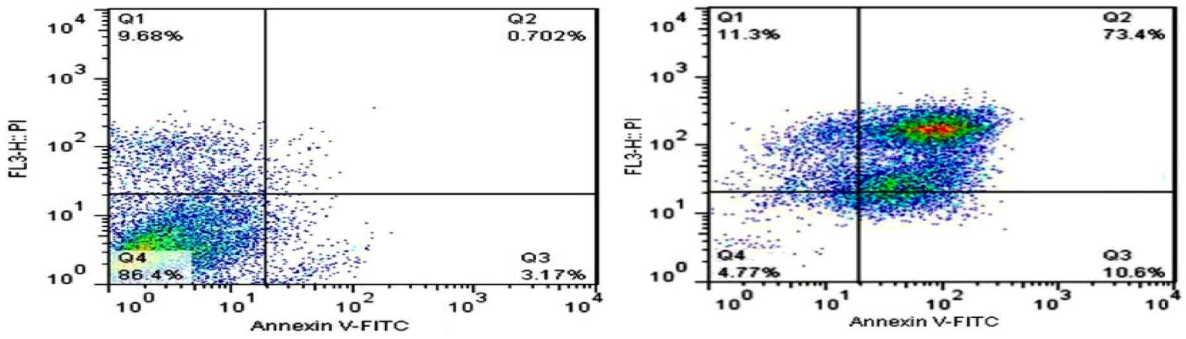

Figure 9. Effect of M4 on apoptosis assay from cancer cell PC3. (A) Untreated prostate cancer cell PC3 (Control). (B)The effect of the IC_{50} concentration of the amide thiazolidine on apoptosis of prostate cancer PC-3.

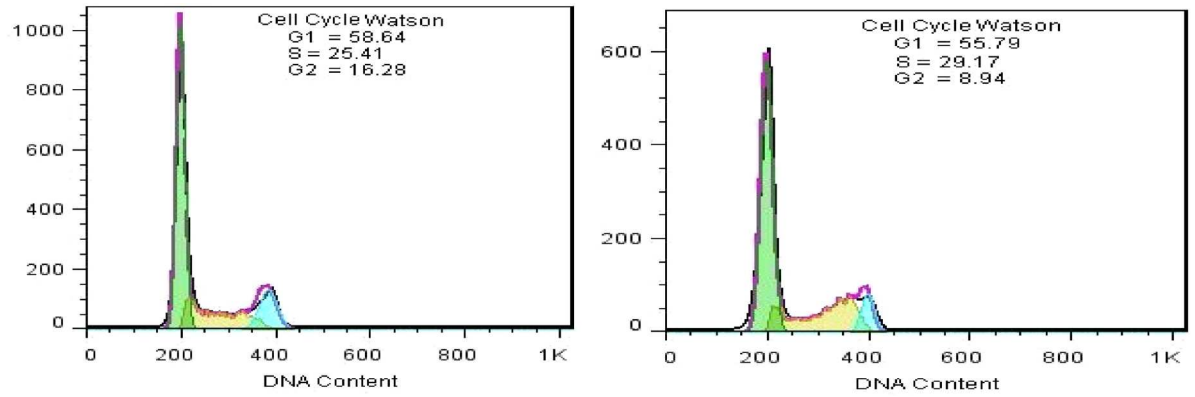

Figure 10. Effect of compound M4 on cell cycle assay in cancer cells: (A) Control prostate cancer cell PC3. (B) Effect of amide thiazolidine M4 on the cell cycle of PC3.

early apoptosis Q2, and late programed death Q3). It was observed that the percentage of live cancer cells Q4 significantly decreased to 4.77% compared to 86.4% in the control after treatment with the active compound.

Additionally, there was a high apoptosis rate in Q2 cells at 73.4% and early late apoptosis in Q3 cells at 10.6%, as shown in Figure 7. This illustrates the ability of the amide compound M4 to kill cancer cells by inducing cell aggregation and chromatin shrinkage and its effect on the cytoplasm of the cells, leading to the formation of bodies for cell death. These findings suggest promising effectiveness, indicating the potential future use of the compound as a drug [15].

3.4.4. Effect of M4 on cell cycle analysis

Apoptosis controls the cell cycle and plays a crucial role in developing and spreading cancer cells. Any interruption of the cell cycle at any stage is considered to lead to the cessation and death of cancer cells. The cell cycle consists of important phases: G0, when cells are at rest; G1, representing the synthesis of mRNAs and proteins necessary for DNA replication in the S phase; and G2, where DNA replication is monitored to ensure cell integrity and ability to divide [15, 47]. Cell cycle analysis was performed using a flow cytometer to determine the cytotoxic activity and the effect of the compound M4 at the IC_{50} concentration (Figure 10). It was observed that the cell cycle was arrested at the interphase, with a decrease in the percentage of DNA content to 55.79% in the G1 phase compared to 58.64% in the control and a decrease in the percentage of DNA content in the G2 phase to 8.94%.

Additionally, there was an increase in the percentage of DNA content in the S phase to 29.7%. These changes indicated cell cycle arrest and subsequent cell death, as depicted in Figure 7. The toxic and lethal effect of amide thiazolidine derivatives on PC3 cancer cells is attributed to their direct inhibition of the phosphatidylinositol-3-kinase (PI3 K/AKT) pathway and activation of the 5-AMP protein kinase (AMPK) pathway, leading to programed cell death. Literature suggests that the P21 protein, an inhibitor of cyclin-dependent kinase enzymes and a key member of the Cip/Kip group, plays a crucial role in inhibiting and controlling the cell cycle, thus regulating the proliferation of negative cells and halting them [15,47].

3.5. Computational toxicity study

The cytotoxicity of the active bis amide thiazolidine compound (M4) was assessed using computer-based measurements classified according to international research standards. This classification system provides gradations in the toxicity levels of the studied compounds. The compound M4 was theoretically analyzed, and its results aligned with the International Classification of Organic Compounds. According to this classification, toxicity levels are categorized as follows: the first level is very highly toxic (1 mg/kg or less); the second level is highly toxic (1–50 mg/kg); the third level is moderately toxic (50–500 mg/kg); the fourth level is nontoxic (500–2000mg/kg); and the fifth level is nontoxic (2000–5000 mg/kg).

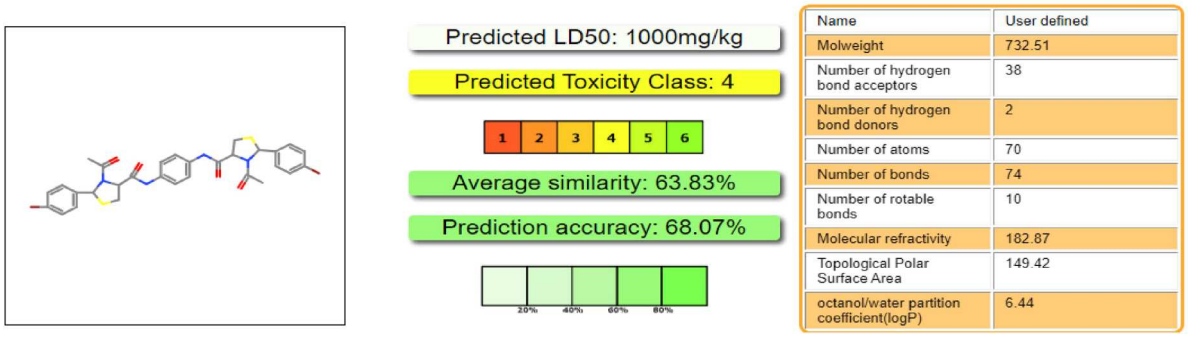

Name	User defined
Molweight	732.51
Number of hydrogen bond acceptors	38
Number of hydrogen bond donors	2
Number of atoms	70
Number of bonds	74
Number of rotable bonds	10
Molecular refractivity	182.87
Topological Polar Surface Area	149.42
octanol/water partition coefficient(logP)	6.44

Figure 11. Cytotoxicity of the active compound M4 was assessed using ProTox-II webserver[41].

Compound M4 demonstrated toxicity within the fourth level, indicating that it is a nontoxic organic compound, as illustrated in Figure 11. Also, studied primitive cytotoxicity using the traditional method and experimented with freshly drowned blood cells and using compounds (M1-M5) at high concentrations (1000, 500, 250, 100, and 50 ppm) and proved that the prepared compounds do not affect red blood cell [47, 48]

4. Conclusion

Herein, bis thiazolidine amides were obtained by reacting aromatic aldehydes with L-cysteine to synthesize thiazolidine, followed by treatment with acetic anhydride. Subsequently, the resulting product was reacted with phenylenediamine to produce bisthiazolidine amide derivatives. These compounds exhibited significant efficacy against both bacteria and prostate cancer cells. Their effectiveness in inducing cell apoptosis and affecting the cell cycle at IC_{50} was also investigated. The newly synthesized molecules were designed theoretically and docked into the androgen receptor and EGFR active sites, revealing that these compounds could not get into the active site of the androgen receptor and showed a good docking score against the EGFR kinase domain, which may indicate that their mechanism of action involves the inhibition of EGFR rather than AR. All thiazolidine amide compounds demonstrated potent biological activity against various bacterial strains (*S. aureus, E. Coli, S. mutans*). Additionally, all compounds exhibited high effectiveness against PC3 cancer cells, with M4 being the most effective compound, showing significant inhibition with an IC_{50} value of 32 µg/ML. M4 was observed to trigger cancer cell death by causing chromatin condensation, altering the cytoplasm, and generating structures associated with cell death suggesting it is using potential as a future drug. The cytotoxicity of M4 was theoretically studied, revealing it as a nontoxic organic compound based on international classification. The toxic effect on PC3 cancer cells was attributed to its inhibition of the phosphatidylinositol-3-kinase (PI3 K/AKT) pathway, activation of the 5-AMP protein kinase (AMPK) pathway, and induction of programed cell death. While our study demonstrates promising biological activity of the bisthiazolidine amide derivatives, further separation and biological evaluation of both diastereomers (trans, cis) are required. Additionally, experimental validation through comprehensive proteomic and kinase profiling assays is essential to confirm target, eliminate potential off-target effects using western plot assays and investigate the inhibition of PI3 K and AKT kinase activity also assess gene expression levels of key downstream targets, including mTOR, S6K1, and Cyclin D1, to confirm pathway inhibition. Further studies, including human evaluations and detailed mechanistic analyses, are warranted to advance these compounds toward clinical applications.

Acknowledgements

The authors express their sincere gratitude to the University of Misan, the University of Basrah, the University of Kufa, and the Ministry of Higher Education and Scientific Research (Iraq) for their invaluable resources, support, and assistance in

the successful completion of this project. Additionally, we appreciate the open access funding generously provided by the University of Vienna.

Author contributions

CRediT: **Sabah Abbas:** Formal analysis, Methodology, Validation, Writing – original draft; **Ahmed A. Majed:** Data curation, Formal analysis, Investigation, Methodology, Software, Validation, Writing – original draft; **Rehab G. Abood:** Data curation, Investigation, Methodology, Writing – original draft; **Dunya AL-Duhaidahawi:** Data curation, Investigation, Methodology, Validation, Visualization, Writing – original draft; **Radwan Alanjjar:** Data curation, Formal analysis, Investigation, Supervision, Visualization, Writing – original draft; **Huda Hadi Nameh:** Formal analysis, Investigation, Methodology, Writing – original draft; **Naser A. Naser:** Data curation, Formal analysis, Investigation, Validation, Visualization, Writing – original draft; **Ahmed Y. Hammood:** Formal analysis, Investigation, Methodology, Validation, Writing – original draft; **Mohammad Y. Alfaifi:** Data curation, Formal analysis, Investigation, Resources, Validation, Writing – original draft; **Ali A. Shati:** Data curation, Funding acquisition, Investigation, Validation, Writing – original draft; **Serag Eldin I. Elbehairi:** Data curation, Formal analysis, Investigation, Software, Validation, Writing – original draft; **Ahmed M. Hussein:** Conceptualization, Data curation, Investigation, Project administration, Software, Validation, Writing – original draft, Writing – review & editing; **Mohammed Aufy:** Data curation, Investigation, Methodology, Validation, Writing – original draft.

Disclosure statement

No potential conflict of interest was reported by the authors.

Funding

The authors gratefully acknowledge the Deanship of Research and Graduate Studies at King Khalid University for funding this work through a Large Research Project grant (No. RGP.1/330/45).

Data availability statement

The data supporting this study's findings are available from the corresponding authors upon reasonable request.

References

[1] Liu, D.; Kuai, Y.; Zhu, R.; Zhou, C.; Tao, Y.; Han, W.; Chen, Q. Prognosis of Prostate Cancer and Bone Metastasis Pattern of Patients: A SEER-Based Study and a Local Hospital Based Study from China. *Sci. Rep* 2020**,** *10*, 9104. https://pubmed.ncbi.nlm.nih.gov/32499554/.

[2] Feng, Z.; Yanbing, D.; Fangyuan, C.; Meng, N.; Ziyang, L.; Chenci, W. Cinobufotalin Capsule Combined with Zoledronic Acid in the Treatment of Pain Symptoms and Clinical Efficacy in Prostate Cancer Patients with Bone Metastases: A Retrospective Study. *Archivos Españoles de Urología* 2024**,** *77* (3), 242–248. DOI: 10.56434/j.arch.esp.urol.20247703.32.

[3] Han, D.; Li, X.; Cheng, Y. Transcription Factor ELF1 Modulates Cisplatin Sensitivity in Prostate Cancer by Targeting MEIS Homeobox 2. *Chemical Research Toxicology* 2023, *36*, 360–368. doi:10.1021/acs.chemrestox.2c00233.

[4] Chia, C.S.B. Novel PSMA-Targeting Radionuclide Peptidomimetics for Treating Prostate Cancer. *ACS Medicinal Chemistry Letters*. 2022, *14* (1), 3–4. DOI: 10.1021/acsmedcheMLett.2c00510.

[5] Denmeade, S.R.; Isaacs, J.T. A History of Prostate Cancer Treatment. *Nat. Rev. Cancer* 2002**,** *2*, 389–396. DOI: 10.1038/nrc801.

[6] Hashemi, M.; Zandieh, M.A.; Talebi, Y.; Rahmanian, P.; Shafiee, S.S.; Nejad, M.M.; Babaei, R.; Sadi, F.H.; Rajabi, R.; Abkenar, Z.O. Paclitaxel and Docetaxel Resistance in Prostate Cancer: Molecular Mechanisms and Possible Therapeutic Strategies. *Biomedicine Pharmacotherapy* 2023**,** *160*, 114392. doi:10.1016/j.biopha.2023.114392.

[7] Obaid, U.R.; Zain, A.N.; Eeshal, F.; Umar, A.; Hiba, I.; Ali, H.; Arsalan, N.; Waqas, R. The Efficacy of Ketoconazole Containing Regimens in Castration-Resistant Prostate Cancer: A Systematic Review and Meta-Analysis. *Clin. Genitourin Cancer* 2024, *22* (2), 483–490. doi:10.1016/j.clgc.2024.01.003.

[8] He, Y.; Xu, W., Xiao, Y.T., et al. Targeting Signaling Pathways in Prostate Cancer: Mechanisms and Clinical Trials. *Sig Transduct Target Ther* 2022, *7*, 198. https://pubmed.ncbi.nlm.nih.gov/35750683/.

[9] Yao, X.; Zhu, Y.; Huang, Z.; Wang, Y.; Cong, S.; Wan, L., … Hu, Z. Fusion of Shallow and Deep Features from 18F-FDG PET/CT for Predicting EGFR-Sensitizing Mutations in non-Small Cell Lung Cancer. *Quant. Imaging. Med. Surg.* 2024, *14* (8), 5460–5472. doi:10.21037/qims-23-1028.

[10] Tahseen, S.F.A.; Hamid, M.S.A.; Ahmed, A.M.; Mustafa, H.M.; Eman, S.; Radwan, A. Synthesis, Breast Cancer Activity, Molecular Docking and Dynamic Simulation of 1,4-Dihydropyridine Derivatives. *J. Mol. Struct.* 2025, *1321*. https://www.sciencedirect.com/science/article/abs/pii/S0022286024022142.

[11] Suresh, S.; Huard, S.; Dubois, T. CARM1/PRMT4: Making Its Mark Beyond its Function as a Transcriptional Coactivator. *Trends Cell Biol.* 2021**,** *31*, 402–417. DOI: 10.1016/j.tcb.2020.12.010.
[12] Al-Hujaj, H.H.; Majed, A.A.; Qeaser, R.A.; Dawood, S.A.; Noor, H.F.; Huda, H.N.; Naser, A.N.; Magdi, E.A.Z.; Sami, A.A.; Sobhi, M.G.; Anas, A.; Ahmed, A.E.; Islam, M.A. Thiazolidine Derivatives as Promising Prostate Cancer Agents: Design, Synthesis, In Vitro Evaluation, DFT, ADME, POM, Docking, and Toxicity Studies. *J. Mol. Struct.* 2025, *1340*, 142544. doi:10.1016/j.molstruc.2025.142544.
[13] Rehab, G.A.; Heider, A.A.; Sabah, A.; Ahmed, A.M.; Ahmed, A.A.; Ayat, A.; Tahseen, A.A. Anti-breast Cancer Potential of new Indole Derivatives: Synthesis, in-Silico Study, and Cytotoxicity Evaluation on MCF-7 Cells. *J. Mol. Struct.* 2025, *1326*, 141176. doi:10.1016/j.molstruc.2024.141176.
[14] Alici, E.H.; Bilgiçli, A.T.; Günsel, A.; Arabaci, G.; Yarasir, M.N. α-Substituted Phthalocyanines Based on Metal-Induced H-or J-Type Aggregation for Silver and Palladium Ions: Synthesis, Fluorescence, and Antimicrobial and Antioxidant Properties. *Dalton Trans.* 2021**,** *50*, 3224–3239. doi:10.1039/D0DT04103C.
[15] Hafez, D.E.; Hafez, E.; Eddiasty, I.; Shih, S.-P.; Chien, L.-C.; Hong, Y.-J.; Lin, H.-Y.; Keeton, A.B.; Piazza, G.A.; Abdel-Halim, M. Novel Thiazolidine Derivatives as Potent Selective pro-Apoptotic Agents. *Bioorg. Chem.* 2021**,** *114*, 105143. doi:10.1016/j.bioorg.2021.105143.
[16] Ghosh, A.K.; Brindisi, M.; Sarkar, A. The Curtius Rearrangement: Applications in Modern Drug Discovery and Medicinal Chemistry. *ChemMedChem* 2018**,** *13*, 2351–2373. doi:10.1002/cmdc.201800518.
[17] Chavarria, D.; Silva, T.; Magalhães e Silva, D.; Remião, F.; Borges, F. Lessons from Black Pepper: Piperine and Derivatives Thereof. *Expert Opin. Ther. Pat.* 2016**,** *26*, 245–264. DOI: 10.1517/13543776.2016.1118057.
[18] Tessoulin, B.; Papin, A.; Gomez-Bougie, P.; Bellanger, C.; Amiot, M.; Pellat-Deceunynck, C.; Chiron, D. BCL2-Family Dysregulation in B-Cell Malignancies: From Gene Expression Regulation to a Targeted Therapy Biomarker. *Front. Oncol.* 2019, *8*, 645. doi:10.3389/fonc.2018.00645.
[19] Elimam, D.M.; Elgazar, A.A.; El-Senduny, F.F.; El-Domany, R.A.; Badria, F.A.; Eldehna, W.M. Natural Inspired Piperine-Based Ureas and Amides as Novel Antitumor Agents Towards Breast Cancer. *J. Enzyme Inhib. Med. Chem.* 2022, *37*, 39–50. doi:10.1080/14756366.2021.1988944.
[20] Xu, S.; Jiang, J.; Qi, Y.; Ding, X.; Wu, Y.; Lei, H.; Zhao, Y. Design and Synthesis of Biaryloxazolidinone Derivatives Containing Amide or Acrylamide Moiety as Novel Antibacterial Agents Against Gram – Positive Bacteria. *Bioorg. Med. Chem. Lett.* 2019, *29*, 126747. doi:https://doi.org/10.1016j.bmcl.2019.126747.
[21] Kabir, E.; Uzzaman, M. A Review on Biological and Medicinal Impact of Heterocyclic Compounds. *Results in Chemistry* 2022**,** *4*, 100606. doi:10.1016/j.rechem.2022.100606.
[22] Naim, M.J.; Alam, M.J.; Ahmad, S.; Nawaz, F.; Shrivastava, N.; Sahu, M.; Alam, O. Therapeutic Journey of 2, 4-Thiazolidinediones as a Versatile Scaffold: An Insight Into Structure Activity Relationship. *Eur. J. Med. Chem.* 2017, *129*, 218–250. DOI: 10.1016/j.ejmech.2017.02.031.
[23] Mahapatra, D.K.; Asati, V.; Bharti, S.K. Chalcones and Their Therapeutic Targets for the Management of Diabetes: Structural and Pharmacological Perspectives. *Eur. J. Med. Chem.* 2015**,** *92*, 839–865. DOI: 10.1016/j.ejmech.2015.01.051.
[24] A.Majed, A.; Al-Duhaidahawi, D.; Omran, A.; Abbas, H.; Abid, S.; Hmood, D.S.D.S. Synthesis, Molecular Docking of new Amide Thiazolidine Derived from Isoniazid and Studying Their Biological Activity Against Cancer Cells. *J. Biomol. Struct. Dyn.* 2023, *42*, 13485–13496. DOI: 10.1080/07391102.2023.2276313.
[25] Venkata, S.R.G.; C. Narkhede, U.; Jadhav, V.D.; Naidu, C.G.; Addada, R.R.; Pulya, S.; Ghosh, B. Quinoline Consists of 1H-1, 2, 3-Triazole Hybrids: Design, Synthesis and Anticancer Evaluation. *Chemstry Select* 2019**,** *4* (48), 14184–14190. DOI:10.1002/slct.201903938.
[26] Osmaniye, D.; Levent, S.; Ardıç, C.M.; Atlı, Ö; Özkay, Y.; Kaplancıklı, Z.A. Synthesis and Anticancer Activity of Some Novel Benzothiazole-Thiazolidine Derivatives. *Phosphorus, Sulfur Silicon Relat. Elem.* 2017**,** *193* (4), 249–256. DOI:10.1080/10426507.2017.1395878.
[27] Al-Mathkuri, T.S.F.; Majed, A.A.; Emshary, C.A.; Hassan, Q.M.A.; Dhumad, A.M.; Abid, D.S. Synthesis, DFT Study and Optical Nonlinear Evaluations of a new 1,3,4 – Oxadiazole Derivative. *J. Indian Chem. Soc.* 2025**,** *102*, 101841. doi:10.1016/j.jics.2025.101841.
[28] Almalki, A.S.; Nazreen, S.; Malebari, A.M.; Ali, N.M.; Elhenawy, A.A.; Alghamdi, A.A.; Ahmad, A.; Alfaifi, S.Y.; Alsharif, M.A.; Alam, M.M. Synthesis and Biological Evaluation of 1, 2, 3-Triazole Tethered Thymol-1, 3, 4-Oxadiazole Derivatives as Anticancer and Antimicrobial Agents. *Pharmaceuticals* 2021**,** *14*, 866. doi:10.3390/ph14090866.
[29] Trotsko, N.; Kosikowska, U.; Paneth, A.; Plech, T.; Malm, A.; Wujec, M. Synthesis and Antibacterial Activity of new Thiazolidine-2, 4-Dione-Based Chlorophenylthiosemicarbazone Hybrids. *Molecules* 2018, *23*, 1023. DOI: 10.3390/molecules23051023.
[30] Abdelgawad, M.A.; El-Adl, K.; El-Hddad, S.S.A.; Elhady, M.M.; Saleh, N.M.; Khalifa, M.M.; Khedr, F.; Alswah, M.; Nayl, A.A.; Ghoneim, M.M.; Abd El-Sattar, N.E.A. Design, Molecular Docking, Synthesis, Anticancer and Anti-Hyperglycemic Assessments of Thiazolidine-2,4-Diones Bearing Sulfonylthiourea Moieties as Potent VEGFR-2 Inhibitors and PPARγ Agonists. *Pharmaceuticals* 2022, *15*, 226. doi:10.3390/ph15020226.
[31] Majed, A.A.; Abid, D.S. Synthesis of Some New Thiazolidine and 1, 3, 4-Oxadiazole Derived from L-Cysteine and Study of Their Biological Activity as Antioxidant and Breast Cancer. *Letters in Applied NanoBioScience* 2023, *12*, 82. doi:10.33263/LIANBS123.082.

[32] Qiu, Z.; Hongyu, Z.; Shumei, Z.; Bing, Y. Natural Product-Inspired Synthesis of Thiazolidine and Thiazolidinone Compounds and Their Anticancer Activities. *Curr. Pharm. Des.* 2010, *16* (16), 1826–1842. doi:10.2174/138161210791208983.
[33] Donia, E.H.; Eman, H.; Islam, E.; Shou-Ping, S.; Leng-Chiang, C.; Yi-Jia, H.; Hung-Yu, L.; Adam, B.K.; Gary, A.P.; Mohammad, A.; Ashraf, H.A. Novel Thiazolidine Derivatives as Potent Selective pro-Apoptotic Agents. *Bioorg. Chem.* 2021, *114*, 105143. doi:10.1016/j.bioorg.2021.105143.
[34] Zhu, J.; Jiang, X.; Luo, X.; Zhao, R.; Li, J.; Cai, H.; Ye, X.; Bai, R.; Xie, T. Combination of Chemotherapy and Gaseous Signaling Molecular Therapy: Novel β-Elemene Nitric Oxide Donor Derivatives Against Leukemia. *Drug Dev. Res.* 2023**,** *84* (4), 718–735. doi:10.1002/ddr.22051.
[35] Blanquicett, C.; Roman, J.; Hart, C.M. Thiazolidinediones as Anti-Cancer Agents. *Cancer. Ther.* 2008, *6*, 25–34.
[36] Galbraith, L.C.A.; Mui, E.; Nixon, C.; Hedly, A.; Strachan, D.; Mackay, D.; Sansom, O.J.; Leung, H.Y.; Ahmed, I. PPAR-gamma Induced AKT3 Expression Increases Levels of Mitochondrial Biogenesis Driving Prostate Cancer. *Oncogene* 2021**,** *40*, 2355–2366. doi:10.1038/s41388-021-01707-7.
[37] Elancheran, R.; Saravanan, K.; Divakar, S.; Kumari, S.; Maruthanila, V.L.; Kabilan, S.; Ramanathan, M.; Devi, R.; Kotoky, J. Design, Synthesis and Biological Evaluation of Novel 1, 3 – Thiazolidine-2, 4-Diones as Anti-Prostate Cancer Agents. *Anti-Cancer Agents Med. Chem.* 2017**,** *17* (13), 1756–1768. doi:10.2174/1871521409666170412121820.
[38] Veeresa, G.; Eunju, H.; Sullivan, J.; Dalton, J.T.; Miller, D.D. SAR Studies of 2-Arylthiazolidine-4-Carboxylic Acid Amides: A Novel Class of Cytotoxic Agents for Prostate Cancer. *Bioorg. Med. Chem. Lett.* 2005, *15* (18), 4010–4013. doi:10.1016/j.bmcl.2005.06.032.
[39] Lu, Y.; Li, C.-M.; Yang, X.; Ross, C.A.; Chen, J.; Dalton, J.T.; Li, W.; Miller, D.D. Discovery of 4-Substituted Methoxybenzoyl-Aryl-Thiazole as Novel Anticancer Agents: Synthesis, Biological Evaluation, and Structure −Activity Relationships. *J. Med. Chem.* 2009, *52* (6), 1701–1711. doi:10.1021/jm801449a.
[40] Hafez, D.E.; Hafez, E.; Eddiasty, I.; Shih, S.-P.; Chien, L.-C.; Hong, Y.-J.; Lin, H.-Y.; Keeton, A.B.; Piazza, G.A.; Abdel-Halim, M.; Abadi, A.H. Novel Thiazolidine Derivatives as Potent Selective Pro-Apoptotic Agents. *Bioorg. Chem.* 2021**,** *114* (11), 105143. doi:10.1016/j.bioorg.2021.105143.
[41] Song, Z.-C.; Ma, G.-Y.; Zhu, H.-L. Synthesis, Characterization and Antibacterial Activities of N-Tert-Butoxycarbonyl-Thiazolidine Carboxylic Acid. *RSC Adv.* 2015**,** *5*, 24824–24833. doi:10.1039/C4RA15284K.
[42] Ahmed, A. M.; Qeaser, R. A.; Hamsa, H. A.; Dawood S. A.; Abdulaziz A. A.; Islam M. A.; Ahmed A. E.; Synthesis, Characterization, Bioactivity Evaluation, and POM/DFT/Docking Analysis of Novel Thiazolidine Derivatives as Potent Anticancer and Antifungal Agents. *Chemistry Select*. 2024, 9, 40, e202403761. doi:10.1002/slct.202403761
[43] Haider, A.O.; Ahmed, A.M.; Kawkab, H.; Dawood, S.A.; Mostafa, A.A.; Ahmed, E.; Mohamed, H.K.; Mohamed, A. Anti-Cancer Activity. DFT and Molecular Docking Study of new BisThiazolidine Amide. *Results in Chemistry* 2024**,** *12*, 101835. doi:10.1016/j.rechem.2024.101835.
[44] Zhang, L.; Shi, H.; Tan, X.; Jiang, Z.; Wang, P.; Qin, J. Ten-gram-scale Mechanochemical Synthesis of Ternary Lanthanum Coordination Polymers for Antibacterial and Antitumor Activities. *Front. Chem.* 2022**,** *10*, 898324. doi:10.3389/fchem.2022.898324.
[45] Naz, S.; Al Kury, L.T.; Nadeem, H.; Shah, F.A.; Ullah, A.; Paracha, R.Z.; Imran, M.; Li, S. Synthesis, In Silico and Pharmacological Evaluation of New Thiazolidine-4-Carboxylic Acid Derivatives Against Ethanol-Induced Neurodegeneration and Memory Impairment. *J. Inflamm. Res.* 2022, 3643–3660. https://www.sciencedirect.com/science/article/abs/pii/S0022286024022142.
[46] Garza, I.; Wallace, M.J.; Fernando, D.; Singh, A.; Lee, R.E.; Gerding, J.S.; Franklin, C.; Yendapally, R. Synthesis and Evaluation of Thiazolidine Amide and N-Thiazolyl Amide Fluoroquinolone Derivatives. *Arch. Pharm.* 2017**,** *350*, e201700029. doi:10.1002/ardp.201700029.
[47] Beharry, Z.; Zemskova, M.; Mahajan, S.; Zhang, F.; Ma, J.; Xia, Z.; Lilly, M.; Smith, C.D.; Kraft, A.S. Novel Benzylidene-Thiazolidine-2, 4-Diones Inhibit Pim Protein Kinase Activity and Induce Cell Cycle Arrest in Leukemia and Prostate Cancer Cells. *Mol. Cancer Ther.* 2009**,** *8*, 1473–1483. doi:10.1158/1535-7163.MCT-08-1037.
[48] Banerjee, P.; Eckert, A.O.; Schrey, A.K.; Preissner, R. ProTox-II: A Webserver for the Prediction of Toxicity of Chemicals. *Nucleic Acids Res.* 2018, *46*, W257–W263. doi:10.1093/nar/gky318.
[49] Wadi, J.S.; Dunya, A.D.; Jabir, M.; Najim, M.A.; Jawad, S.F.; Hamzah, S.S.; Qais, F.A. Exploring the Interaction Between 3-D Structure of TLR 9 and Prostaglandin Analogues. *Arabian Journal of Chemistry* 2023**,** *16*, 104692. doi:10.1016/j.arabjc.2023.104692.
[50] Wadi, J.; Sagheer, O. Mulberroside A Could Serve as a Pan Inhibitor for the Tyrosine Kinase Domains of the HER Family. *F1000Res* 2022**,** *11*, 1201. https://f1000research.com/articles/11-1201.
[51] Al-Kelabi, H.; Al-Duhaidahawi, D.; Al-Khafaji, K.; Al-Masoudi, N.A. New Tamoxifen Analogs for Breast Cancer Therapy: Synthesis, Aromatase Inhibition and *In silico* Studies. *J. Biomol. Struct. Dyn.* 2023**,** *41*, 12798–807. doi:10.1080/07391102.2023.2175375.